CHINESE OPTICS LETTERS

Vol. 22, No. 5 | May 2024

Robust thin-film lithium niobate modulator on a silicon substrate with backside holes

Mai Wang (王 迈)[1], Lu Qi (祁 璐)[2,3], Haohua Wang (王浩华)[2,3], Ziliang Ruan (阮子良)[1], Gengxin Chen (陈耿鑫)[1], Bin Chen (陈 斌)[1], Shengqi Gong (龚胜琪)[1], Kaixuan Chen (陈楷旋)[2,3], and Liu Liu (刘 柳)[1,4*]

[1] State Key Laboratory of Extreme Photonics and Instrumentation, College of Optical Science and Engineering, International Research Center for Advanced Photonics, Zhejiang University, Hangzhou 310058, China

[2] Guangdong Provincial Key Laboratory of Optical Information Materials and Technology, South China Academy of Advanced Optoelectronics, South China Normal University, Higher-Education Mega-Center, Guangzhou 510006, China

[3] National Center for International Research on Green Optoelectronics, South China Normal University, Guangzhou 510006, China

[4] Jiaxing Key Laboratory of Photonic Sensing & Intelligent Imaging, Intelligent Optics & Photonics Research Center, Jiaxing Research Institute, Zhejiang University, Jiaxing 314000, China

*Corresponding author: liuliuopt@zju.edu.cn

Received November 11, 2023 | Accepted January 15, 2024 | Posted Online May 14, 2024

Recently, Mach–Zehnder modulators based on thin-film lithium niobate have attracted broad interest for their potential for high modulation bandwidth, low insertion loss, high extinction ratio, and high modulation efficiency. The periodic capacitively loaded traveling-wave electrode is optimally adopted for ultimate high-performances in this type of modulator. However, such an electrode structure on a silicon substrate still suffers from the velocity mismatch and substrate leakage loss for microwave signals. Here, we introduce a thin-film lithium niobate modulator structure using this periodic capacitively loaded electrode on a silicon substrate. Backside holes in the silicon substrate are prepared to solve robustly the above difficulties. The fabricated device exhibits an insertion loss of 0.9 dB, a halfwave-voltage–length product of 2.18 V·cm, and an ultra-wide bandwidth well exceeding 67 GHz for a 10-mm-long device. Data transmissions with rates up to 112 Gb/s are demonstrated. The proposed structure and fabrication strategy are compatible for other types of monolithic and heterogeneous integrated thin-film lithium niobate modulators on a silicon substrate.

Keywords: lithium niobate; electro-optic modulator; high bandwidth; backside holes; robust structure.
DOI: 10.3788/COL202422.050601

1. Introduction

In the past few decades, lithium niobate materials have been adopted for their linear electro-optic (EO) effects, wide transparent windows, excellent temperature stability, and stable chemical and physical properties[1]. This renders the lithium niobate-based light modulator one of the most successful optoelectronic devices in commercial optical communication applications[2]. Traditional bulk lithium niobate modulators are based on ion exchange or titanium diffused waveguides[3]. Due to the low light confinement, the drive voltage of such a modulator is generally large, and the EO modulation bandwidth is limited to around 40 GHz. High density on-chip integration with other components is also difficult. Therefore, the bulk lithium niobate modulator cannot meet the increasing requirements in high-density optical interconnect systems. In recent years, thin-film lithium niobate (TFLN) has emerged as a promising platform for highly confined photonic waveguides and devices in lithium niobate[1,4]. TFLN-based modulators with low drive voltages and ultra-high EO bandwidths have recently been demonstrated[5-10].

In order to obtain a large modulation bandwidth for a travelling wave Mach-Zehnder modulator (MZM), both velocity (or effective refractive index) matching between light and microwave signals and impedance matching to common 50 Ω are necessary when designing such a modulator[5,6]. The key modulation efficiency metric, i.e., the half-wave-voltage-length product ($V_\pi L$), is also a key parameter for MZMs. For a given device length, a smaller $V_\pi L$ leads to a smaller half-wave voltage V_π, which favors a low power consumption for modulation. An EO modulator with both a low V_π and a large bandwidth is always desired for applications ranging from digital optical communications to microwave photonic analog links. However, there exists a trade-off between the drive voltage and the modulation bandwidth[11]. The lower V_π is, the longer the device size, and consequently the smaller the bandwidth. To break

the voltage-bandwidth trade-off, periodic capacitively loaded traveling-wave (CLTW) electrodes are introduced in TFLN MZMs on a low permittivity quartz substrate[12,13]. Such a structure was latterly introduced on a silicon substrate as well[14-17]. In order to match the velocities in this case, the silicon substrate was undercut etched from the surface of the wafer[15-17].

In this paper, we demonstrate a TFLN-based EO modulator using the CLTW electrode on a silicon substrate. A new and robust technique by etching holes from the backside of the wafer is introduced to achieve velocity matching. This technique also helps to reduce microwave absorption losses from the semiconducting substrate. The fabricated device exhibits extraordinarily high-frequency performances with bandwidth well exceeding 67 GHz. It also shows a low optical insertion loss of 0.9 dB and a large static extinction ratio of > 20 dB. On-off key (OOK) and four-level pulse-amplitude modulation (PAM-4) up to 112 Gb/s are successfully achieved.

2. Device Design and Fabrication

Figure 1(a) shows a three-dimensional view of the proposed TFLN-based EO modulator. The device uses a classic traveling-wave based MZM structure. It is designed on an x-cut lithium-niobate-on-insulator wafer, which consists of 400 nm TFLN layer, 3 μm thick buried oxide (BOX) layer, and 525 μm thick undoped Si substrate. The TFLN waveguide in the modulation region has a ridge height of 200 nm and a width of 1.5 μm. Multimode interference couplers are used as 3 dB beam splitters/combiners. The modulation electrode utilizes a CLTW design based on a classical coplanar line structure with some periodically loaded T-segments. As compared to conventional traveling-wave electrodes, it has been shown that the CLTW electrode with a much wider signal metal can give much lower microwave losses, while still maintaining a similar modulation efficiency. Therefore, a larger modulation bandwidth can be obtained at the same half-wave voltage V_π. Figures 1(a) and 1(b) show cross-sectional views of the EO modulators. The gap g between the T-segment affects the modulation efficiency of the device. The smaller g is, the stronger the electrical field that can be produced with the same voltage, and therefore the higher the modulation efficiency. However, it should be noted

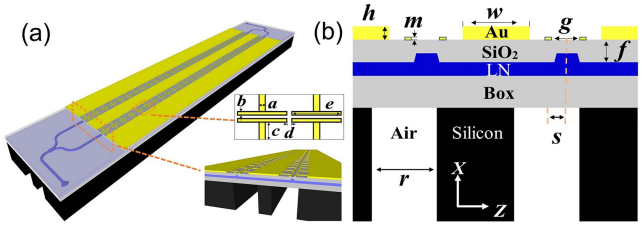

Fig. 1. Proposed TFLN EO modulator with backside holes on a silicon substrate using the CLTW electrode. (a) Three-dimensional views of the whole device and the cross-section at the modulation section. (b) Cross-sectional view of the misaligned device, showing all its structural parameters.

that metal has a strong absorption for light waves, and too close a distance will bring a significant optical propagation loss. After a careful optimization, the electrode metal is designed on top of a SiO_2 over-cladding layer of thickness $f = 900$ nm with an electrode gap $g = 1.8$ μm. In this case, excessive optical losses due to metal are negligible. To ease fabrications, the metal thickness of the T-segments is set to $m = 200$ nm, and the straight signal and ground metals have a thickness of $h = 1.1$ μm. This configuration is also adopted in our previous demonstrations[15]. The signal electrode has a width of $w = 100$ μm, which is wide to ensure a low microwave loss as mentioned above. The so-called slow-wave effect that results from this CLTW electrode would largely affect the index matching required for a travelling-wave modulator. As is shown in Fig. 1(a), here we utilize holes from the backside of the silicon substrate to reduce the microwave refractive index and restore the index matching between the microwave and light. As compared to our previous demonstrations using under-cut holes, this structure is more robust considering fabrications as those discussed below. The rest parameters of the CLTW electrode are designed to guarantee the impedance matching, which gives $(a, b, c, d, e) = (2, 2, 13, 3, 47)$ μm.

We utilize a multi-physics field solver based on a finite element algorithm to simulate the electrical and optical modes of the structure. Through calculation, the half-wave voltage length product $V_\pi L = 2.10\ \text{V} \cdot \text{cm}$ for the fundamental transverse electrical (TE) mode can be obtained, and the optical propagation loss is as low as 0.04 dB/cm due to the metal absorption, as shown in Fig. 2(b). In Fig. 2(a), one can see that the microwave field is also concentrated in the gap between the opposing T-segments electrodes rather than wide signal metal. Consequently, the optical field in the waveguide can have more overlap with the electrical field, and a lower $V_\pi L$ can be obtained. We further analyze the characteristic parameters at different frequencies, which are microwave loss α_m, microwave effective index n_m, and characteristic impedance Z_c, as shown in Figs. 2(c)–2(e), respectively. The microwave loss can be expressed as $\alpha_m = \alpha_0 (f)^{1/2}$, where f is the frequency of the microwave signal and α_0 is the frequency independent characteristic microwave loss. Here, α_0 is extracted as $0.19\ \text{dB}/(\text{cm} \cdot \text{GHz}^{-1/2})$ from the curve in Fig. 2(c), which is similar to the case with the undercut etching[15]. The effects of the backside hole structures on the RF characteristics are further investigated in Fig. 3. As expected, when the width of the hole increases, the microwave effective index n_m decreases. On the other hand, the characteristic impedance Z_c is maintained between 40 Ω and 50 Ω in the whole parameter range in Fig. 3(a). This also indicates that a large tuning range for n_m can be achieved by solely adjusting r while a good impedance matching is maintained. As the group index of the optical wave in the TFLN waveguide is about 2.2, the index matching condition can be fulfilled at $r = 55$ μm. As the holes are defined from the backside of the wafer, we also analyzed the effect of the misalignment of them to the center of the waveguide, which is shown in Fig. 3(b). Indeed, this misalignment would affect n_m, as well as Z_c, slightly. Nevertheless, considering a normal alignment accuracy of 5 μm

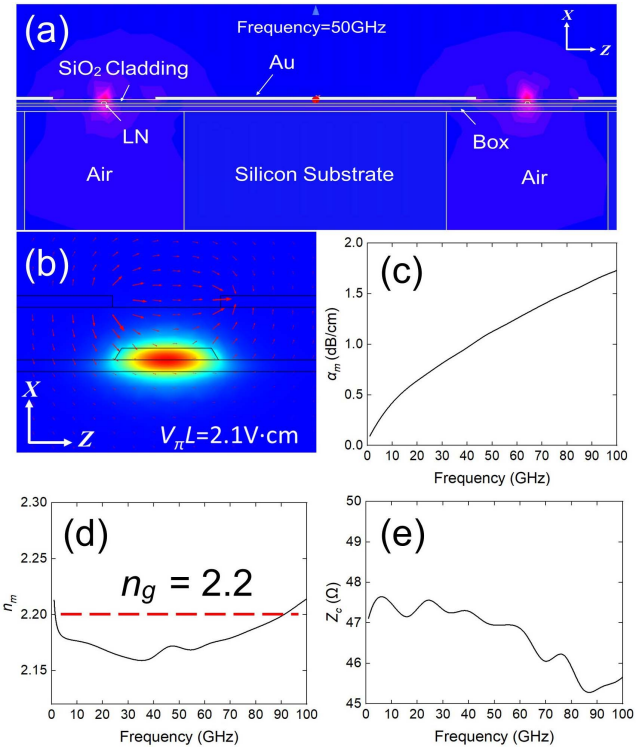

Fig. 2. (a) Simulated RF mode profile at the microwave frequency of 100 GHz. (b) Simulated TE optical mode profile and static electrical field distribution. $V_\pi L$ = 2.10 V·cm can be extracted. Simulated frequency-dependent results of (c) microwave loss α_m, (d) microwave effective index n_m, and (e) characteristic impedance Z_c. The red dashed line in (d) corresponds to the optical group index n_g.

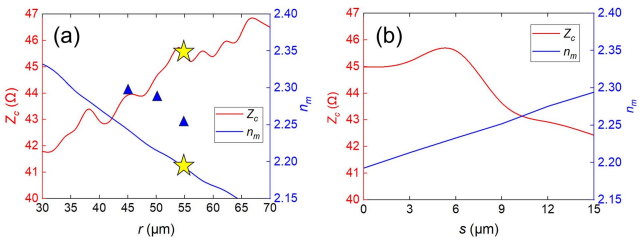

Fig. 3. (a) Effects of the width r of backside holes on Z_c and n_m at 100 GHz. The optimal points (r = 55 μm) adopted in the experiments are marked as yellow stars. The blue triangles are n_m extracted from experiments. (b) Effects of the misalignment s of backside holes on Z_c and n_m when r = 55 μm.

for a double-side mask aligner, the relative change of n_m is still within 1%. This also shows that the proposed structure exhibits a good fabrication tolerance for achieving index matching.

The designed EO modulator was fabricated through a series of standard micro-fabrication processes. First, electron-beam lithography was used to pattern the ma-N 2403 resist on a chip. Then, a 200 nm thick lithium niobate layer was removed using Ar plasma by means of inductively coupled plasma reactive ion etching (ICP-RIE) technology with an etching rate of ~80 nm/min. Next, the chip was covered with a 900 nm thick SiO_2 layer deposited by plasma enhanced chemical vapor

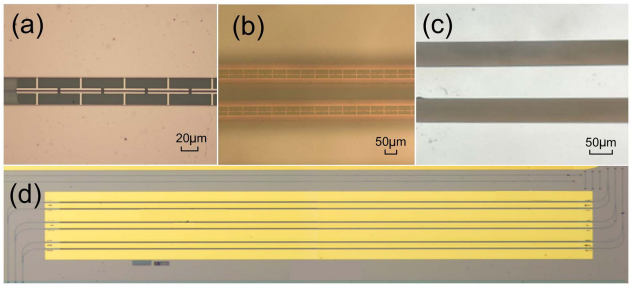

Fig. 4. (a) Top view of partial electrode. Backside view of the device focusing on (b) the electrode and (c) surface of chip backside. (d) Image of the whole fabricated device.

deposition (PECVD). The metal electrodes, made of Au, were prepared using ultra-violet contact lithography, metal evaporation, and lift-off processes. The chip was then thinned to ~200 μm thick by a grinding and polishing machine. Finally, the hole patterns were prepared on the polished backside of the chip using a double-side mask aligner, and anisotropic deep RIE of silicon was performed to remove the silicon substrate beneath the modulation section until the BOX layer. As compared to the previous version of undercut etching from the chip surface[15], the proposed backside hole structure facilitates the fabrication processes in a few aspects. First, it is known that the silicon isotropic dry etching would show a severe loading effect, i.e., the silicon etching speed is largely dependent on the etched area around the structures. It is hard to control the amount of undercut etching accurately. In the proposed approach, the width of the backside holes is the critical parameter as discussed in the simulations, and it can be defined accurately using lithography. Due to the high etching selectivity over SiO_2, the deep silicon etching will also stop naturally on the BOX layer. Secondly, a full membrane structure is produced here, which is mechanically more stable as compared to the bridge structure resulting from the undercut etching from the top. Actually, the present device has gone through a harsh mechanical dicing process without breaking. These render more robust fabrication processes for the proposed modulators. Figure 4 shows some images of the CLTW electrode from the front and the back, as well as the whole fabricated device.

3. Measurement and Analysis

Three devices were prepared with different widths of the backside holes, which are r = 45, 50, and 55 μm, respectively, and the modulation lengths are all 1 cm. A continuous wave laser is used as the input light at 1550 nm wavelength to the device. A polarization controller was employed to ensure the TE polarization input. As shown in Fig. 4(d), a pair of grating couplers (GCs) was prepared to couple light into and out from the chip[18]. The coupling loss can be measured through a reference structure consisting of two GCs connected back-to-back on the chip. As shown in Fig. 5, the half-wave voltage V_π was measured to be 2.18 V, corresponding to a $V_\pi L$ of 2.18 V·cm. This is consistent

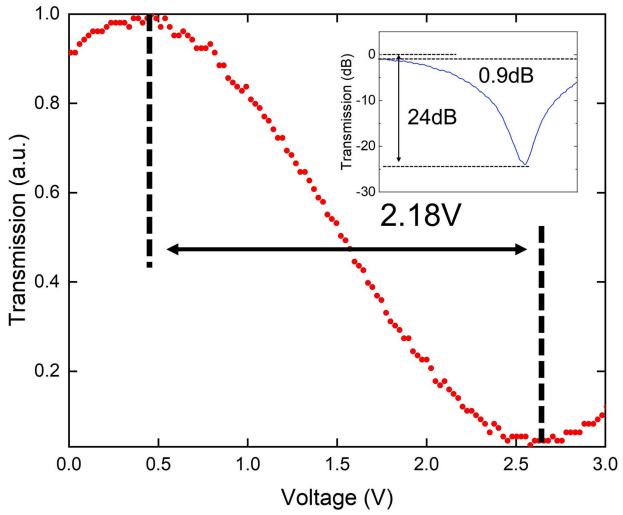

Fig. 5. Normalized optical transmission of the fabricated MZM as a function of the applied voltage. The V_π value is also marked. The inset shows the measured transmissions in a logarithmic scale showing the insertion loss and extinction ratio of the device.

with the simulation results in Fig. 2(b). The total loss of the modulator containing GCs for coupling is measured to be 8.9 dB at the peak coupling wavelength. Considering the coupling loss for one GC of 4 dB, the on-chip insertion loss of the device is 0.9 dB. The extinction ratio was also measured to be 24 dB, which is shown in the inset of Fig. 5.

Then we measured the EO and electric-electric (EE) responses of the fabricated modulators. As is shown in Fig. 6(a), the EE transmission S_{12} indicates a 3.0 dB roll-off at 67 GHz. Furthermore, the EE transmission S_{11} shows that the reflected waves are well below −20 dB over the entire measured frequency range. This indicates that the impedance of the device is matched well with the desired 50 Ω. The microwave losses and indices at

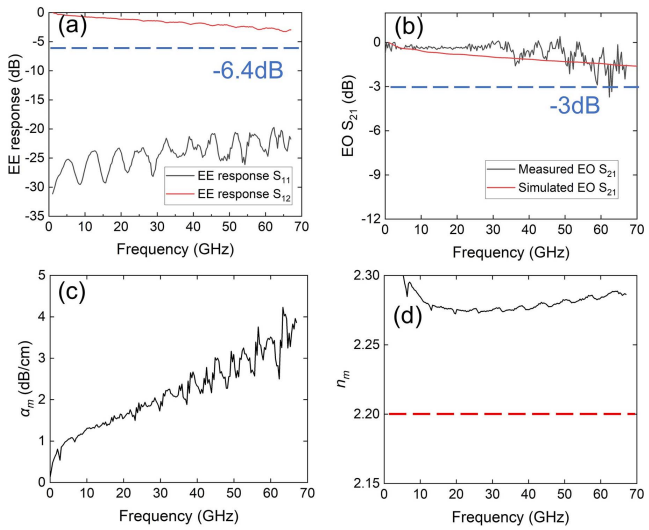

Fig. 6. (a) Measured EE reflection S_{11} and transmission S_{12}. (b) Measured and simulated EO transmission S_{21}. Extracted (c) microwave loss α_m and (d) microwave effective index n_m.

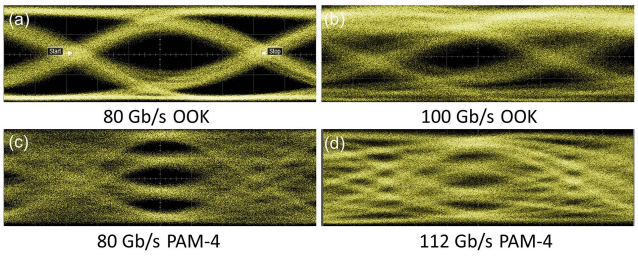

Fig. 7. High-speed data transmissions using the fabricated EO MZM. Measured optical eye diagrams for the OOK format at data rates of (a) 80 Gb/s and (b) 100 Gb/s. Measured optical eye diagrams for the PAM-4 format at data rates of (c) 40 Gbaud (80 Gb/s) and (d) 56 Gbaud (112 Gb/s).

different frequencies were also extracted and are plotted in Figs. 6(c) and 6(d), respectively, where the characteristic microwave loss of $\alpha_0 = 0.4\,\mathrm{dB/(cm \cdot GHz^{-1/2})}$ can be obtained. The microwave losses are about twice as high as those from simulations as mentioned above. The additional microwave losses may come from non-ideally deposited metal and residual silicon under the electrode. The blue triangles in Fig. 3(a) show the measured microwave index n_m of the fabricated devices of $r = 45$, 50, and 55 μm at 67 GHz, which are 2.299, 2.286, and 2.261, respectively. The measured n_m shows slight deviations from those in simulations in Fig. 3. This is partially due to the inaccurate size of the holes on the backside of the chip, as well as the positive sidewall slope from the deep silicon etching, which might result in a narrower silicon opening just beneath the TFLN waveguides. Nevertheless, the results here still indicate that n_m can be controlled effectively by introducing backside holes. The small signal EO responses S_{21} were further measured using a 70 GHz photodetector. As is shown in Fig. 6(b), the EO response shows that the 3 dB bandwidth of the device should well exceed 67 GHz. We then characterized the performance of the device for high-speed data transmissions. Figure 7 shows optical eye diagrams for the OOK modulation at 80 Gb/s and 100 Gb/s and PAM-4 format at 80 Gb/s (40 Gbaud) and 112 Gb/s (56 Gbaud), respectively. It is worthwhile to note that beyond 80 Gbaud the whole measurement system is already limited by its own bandwidth. Nevertheless, open eyes can be observed, which shows the potential for high-speed data transmissions using the proposed device.

4. Conclusion

In conclusion, we have demonstrated a robust TFLN-based EO MZM using the CLTW electrode on a silicon substrate. We used backside holes to solve the problem of velocity mismatch between optical and microwave signals. As compared to the previous undercut etching technique, the present approach facilitates a more robust fabrication process and high modulation performances. Experimentally, the present device has shown a high modulation efficiency $V_\pi L$ of 2.18 V·cm and low optical and microwave losses. The device also had an EO bandwidth well exceeding 67 GHz. The proposed structure and fabrication

strategy can also be readily applied for other types of monolithic and heterogenous integrated thin-film lithium niobate modulators on a silicon substrate.

Acknowledgements

This work was partially supported by the National Natural Science Foundation of China (NSFC) (Nos. 62135012, 62105107, and 61961146003) and Leading Innovative and Entrepreneur Team Introduction Program of Zhejiang (No. 2021R01001)

References

1. A. Boes, L. Chang, C. Langrock, *et al.*, "Lithium niobate photonics: unlocking the electromagnetic spectrum," Science **379**, eabj4396 (2023).
2. E. L. Wooten, K. M. Kissa, A. Yi-Yan, *et al.*, "A review of lithium niobate modulators for fiber-optic communications systems," IEEE J. Sel. Top. Quantum Electron. **6**, 69 (2000).
3. M. De Micheli, J. Botineau, P. Sibillot, *et al.*, "Fabrication and characterization of titanium indiffused proton exchanged (TIPE) waveguides in lithium niobate," Opt. Commun. **42**, 101 (1982).
4. M. G. Vazimali and S. Fathpour, "Applications of thin-film lithium niobate in nonlinear integrated photonics," Adv. Photonics **4**, 034001 (2022).
5. C. Wang, M. Zhang, X. Chen, *et al.*, "Integrated lithium niobate electro-optic modulators operating at CMOS-compatible voltages," Nature **562**, 101 (2018).
6. M. He, M. Xu, Y. Ren, *et al.*, "High-performance hybrid silicon and lithium niobate Mach–Zehnder modulators for 100 Gbit s^{-1} and beyond," Nat. Photonics **13**, 359 (2019).
7. Y. Liu, H. Li, J. Liu, *et al.*, "Low V_π thin-film lithium niobate modulator fabricated with photolithography," Opt. Express **29**, 6320 (2021).
8. M. Xu, Y. Zhu, F. Pittalà, *et al.*, "Dual-polarization thin-film lithium niobate in-phase quadrature modulators for terabit-per-second transmission," Optica **9**, 61 (2022).
9. F. Yang, X. Fang, X. Chen, *et al.*, "Monolithic thin film lithium niobate electro-optic modulator with over 110 GHz bandwidth," Chin. Opt. Lett. **20**, 022502 (2022).
10. G. Chen, Y. Gao, H.-L. Lin, *et al.*, "Compact and efficient thin-film lithium niobate modulators," Adv. Photon. Res. **4**, 2300229 (2023).
11. J. Cai, C. Guo, C. Lu, *et al.*, "Design optimization of silicon and lithium niobate hybrid integrated traveling-wave Mach-Zehnder modulator," IEEE Photonics J. **13**, 2200206 (2021).
12. P. Kharel, C. Reimer, K. Luke, *et al.*, "Breaking voltage–bandwidth limits in integrated lithium niobate modulators using micro-structured electrodes," Optica **8**, 357 (2021).
13. X. Liu, H. Liu, B. Xiong, *et al.*, "Broadband meandered thin-film lithium niobate modulator with ultra-low half-wave voltage," IEEE Photon. Technol. Lett. **34**, 424 (2022).
14. X. Huang, Y. Liu, Z. Li, *et al.*, "Advanced electrode design for low-voltage high-speed thin-film lithium niobate modulators," IEEE Photonics J. **13**, 7900609 (2021).
15. G. Chen, K. Chen, R. Gan, *et al.*, "High performance thin-film lithium niobate modulator on a silicon substrate using periodic capacitively loaded traveling-wave electrode," APL Photonics **7**, 026103 (2022).
16. Y. Xue, R. Gan, K. Chen, *et al.*, "Breaking the bandwidth limit of a high-quality-factor ring modulator based on thin-film lithium niobate," Optica **9**, 1131 (2022).
17. M. Xu, Y. Zhu, J. Tang, *et al.*, "Attojoule/bit folded thin film lithium niobate coherent modulators using air-bridge structures," APL Photonics **8**, 066104 (2023).
18. Z. Ruan, J. Hu, Y. Xue, *et al.*, "Metal based grating coupler on a thin-film lithium niobate waveguide," Opt. Express **28**, 35615 (2020).